Model Order Reduction for Real-Time FPGA-Based Finite Element Transient Simulation of Three-Phase Transformer

Jiuwei Guo, *Student Member, IEEE,* Peng Liu, *Student Member, IEEE,* Venkata Dinavahi, *Fellow, IEEE,* Wenying Yang, *Member, IEEE*

***Abstract*—The finite element method (FEM) is commonly used in modeling the electromagnetic field of transformers with high accuracy; however, the computation time of the FEM is prohibitively high for real-time simulation due to high model order. Reducing the model order is helpful to improve the computational efficiency of the FEM. The proper orthogonal decomposition (POD) is an efficient method to reduce the linear model order but encounters difficulties with nonlinear models. In this paper, a model order reduction (MOR) method based on the combination of POD and the transmission-line modeling (TLM) is proposed to reduce the nonlinear finite element model order and computation time. The TLM method is used to separate the nonlinear components from the model, and then the POD is used to reduce the linear domain order of the model. The nonlinear components obtained by TLM can be solved in parallel on the field programmable gate array (FPGA) to improve computational efficiency further. This paper has studied the transient states of a three-phase transformer with the current excitation and field-circuit coupling. The real-time hardware emulation results are validated by results from offline simulation using Comsol®.**

***Index Terms*—Electromagnetic transient analysis, field programmable gate arrays (FPGAs), finite element method (FEM), model order reduction (MOR), proper orthogonal decomposition (POD), real-time systems, transformers, transmission-line modeling (TLM).**

I. Introduction

TRANSFORMERS are ubiquitous energy conversion equipment essential for AC and DC power transmission and distribution. Commonly observed nonlinear and frequency-dependent events such as inrush currents, faults, ferroresonance, and harmonics impact the power system adversely and can also cause long-term damage to the transformers [1], [2]. Real-time electromagnetic transient simulation can be utilized to predict the impact of such events and devise and test mitigation strategies. Accurate real-time simulation of the transformer requires modeling its electromagnetic field and the field-circuit coupling with the external circuit. The crux of this real-time simulation is to solve the electromagnetic field problem quickly and accurately [3]. Transformers contain nonlinear magnetic materials whose permeability depends on the magnetic field strength, so that the electromagnetic field problems of transformers are typically nonlinear problems. The FEM, as a high accuracy electromagnetic field modeling method, is commonly used for the solution [4], wherein the Newton-Raphson algorithm is used to solve the nonlinear matrix equations in each simulation time-step. The computational effort becomes too high for the simulation if the dimensionality of the matrix system is large due to a large number of FE nodes. The traditional lumped models were used instead of the FEM in many simulations to reduce the computational effort. Useful methods to calculate the leakage inductances have been added into these models to improve the accuracy of the simulation [5]; however, these models become too complex to build when considering the influence of leakage flux and eddy currents [6]–[9], while being unable to provide information about the field distribution and are also less accurate than the FEM.

Field programmable gate arrays (FPGAs) have been effectively utilized for developing detailed device-level real-time models for AC and DC grid equipment [10]. Detailed nonlinear magnetic equivalent circuit based real-time transformer models were also developed on the FPGA [11]. With further hardware development, the parallel FEM algorithms based on hardware devices such as FPGAs and GPUs were also proposed to improve computational efficiency [12]–[14]. However, when the number of FE nodes is large, the computation time is still high because the calculation often cannot be fully parallelized, limited by the computational resources of the FPGA and other hardware devices. In [14], two FPGAs are used for a simple 2D transformer model. It is hard to use the original methods to realize the real-time simulation if the model contains more elements or a 3D model because of the hardware resource limitation.

The main reason for the low computational efficiency is the large matrix system (i.e., the original model order is too high); thus, reducing the finite element model order is necessary to improve the efficiency [15]. There are many model order reduction (MOR) methods that have been widely used in engineering, such as Center Manifold methods, Lyapunov-Schmidt (L-S) methods, Galerkin methods, and proper orthogonal decomposition (POD) methods. Each of them has certain disadvantages and scope of application, as described below:

1) *Center Manifold methods*: Suitable for the case when

This work is supported by Natural Sciences and Engineering Research Council of Canada (NSERC). Jiuwei Guo is supported by China Scholarship Council (CSC) scholarship.

Jiuwei Guo, Wenying Yang, Peng Liu, and Venkata Dinavahi are with the Department of Electrical and Computer Engineering, University of Alberta, Edmonton, Alberta T6G 2V4, Canada. Email: guo_jiuwei@stu.hit.edu.cn, pliu3@ualberta.ca, dinavahi@ualberta.ca, yangwy@hit.edu.cn.

Jiuwei Guo and Wenying Yang are with the Department of Electrical Engineering, Harbin Institute of Technology, Harbin, 150036, China. Corresponding author: Jiuwei Guo.

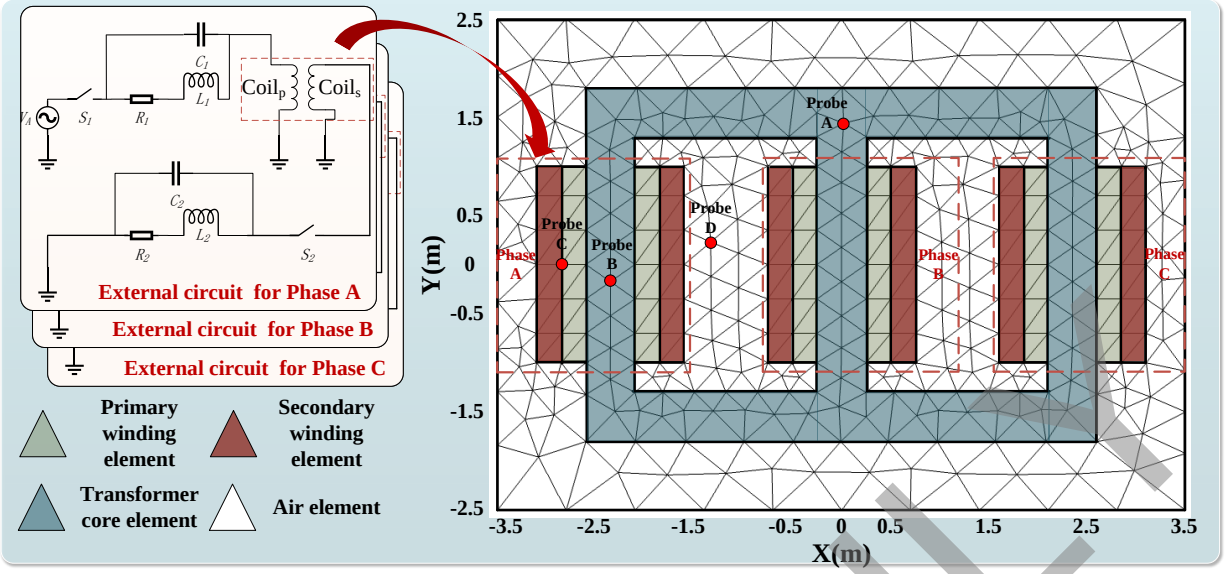

Fig. 1. 2-D FE model of a three-phase transformer with field-circuit coupling .

the original model order is low. For a nonlinear system with higher-order, the order of the new system may still be high [16].

2) *L-S methods*: Suitable for the case when the original model order is low. The low-order nonlinear equations generated by these methods are hard to solve if the original model order is high [17].
3) *Galerkin methods*: These methods are important for large and complex systems; however, it is hard to determine the order number of the low-dimensional model since the error will be large when neglecting too many effects of the high-order model. The inertial manifold theory has been proposed to improve this method, but it is hard to obtain the said manifold in high-order complex systems [18]–[21].
4) *POD methods*: These methods map the high-dimensional model to a low-dimensional model similar to the Galerkin methods [22]; however, these methods use a better orthogonal specification base, and the low-dimensional model order is determined by determining the singular values. They can be seen as improved Galerkin methods, with good performance for FEM simulation [23]–[28].

Although the POD method can be used for the FEM, the state matrix and Jacobian matrices are required to be recalculated during the Newton-Raphson solution process, which costs much time to get these matrices after order reduction. Some interpolation-based POD methods can solve this problem, but the accuracy needs further investigation. Also, because the POD method will change these matrices and break the relationship between these matrices with the finite element nodes, previously proposed parallel algorithms are difficult to be used here.

In this paper, a new MOR method based on the combination of the POD method and the TLM method, i.e., (POD + TLM) is proposed. The TLM theory is valuable in decoupling the nonlinear components of the model from the linear part [29]–[31]. The original FEM model is decoupled by TLM theory into a high-order linear model and several low-order nonlinear components. Then, the linear model is solved by the proposed MOR method, and the nonlinear components are solved in parallel. Because the parallel hardware performance of FPGAs is better in terms of design latency than GPUs and other parallel hardware, the FPGA is the best choice in this paper. Although the FPGA is expensive but compared with the commercial real-time digital simulators it is an affordable choice. The entire POD + TLM methodology for FEM is then emulated on the FPGA to realize the real-time simulation for a three-phase transformer. The proposed method is based on the FEM, so it is also suitable for other cases where FEM can be applied, such as the high frequency transformer.

The paper is organized as follows: in Section II, the POD method and the TLM method are introduced separately. The new method combining the POD and the TLM is also proposed in this section. The field-circuit coupling is explained in Section III. The implementation of the above method on FPGA is presented in Section IV. The case studies of a three-phase power transformer excited by current and external circuits are conducted in Section V. The conclusions are drawn in Section VI.

II. Model Order Reduction for Finite Element Simulation

A. Fundamental FEM Equations

In this paper, a magnetically dynamic problem of a three-phase transformer defined on a 2-D domain is selected as an example, shown in Fig. 1. The structure of this low frequency transformer is simple and symmetrical; therefore, few elements of mesh can guarantee enough accuracy. This mesh has also been used in [12]. In this paper we focus on the difference between the results of the proposed POD method and the FEM. When the transformer working, a magnetic field is produced

in the transformer, which core and surrounding space can be described by the magnetic vector potentials $\mathbf{A}$. The following governing equation can define the problem:

$$\frac{\partial}{\partial x}(\nu\frac{\partial \mathbf{A}}{\partial x})+\frac{\partial}{\partial y}(\nu\frac{\partial \mathbf{A}}{\partial y})=\sigma\frac{\partial \mathbf{A}}{\partial t}-\mathbf{J}, \tag{1}$$

where $\mathbf{J}$ is the impressed current density, ν is the field-dependent magnetic reluctivity, σ is the electrical conductivity. Because the problem is on a 2-D domain (x, y domain), $\mathbf{A}$ and $\mathbf{J}$ only have the z-components.

The FEM solution based on the Galerkin approach is a commonly used method to solve the above problem [32]. The domain is first discretized as shown in Fig. 1. The magnetic vector potentials A^e over the element Ω^e can be interpolated based on the magnetic vector potentials. The vector potentials at the vertices of this element are A_1^e, A_2^e, A_3^e, then the A^e can be obtained by the following equation:

$$A^e=N_1A_1^e+N_2A_2^e+N_3A_3^e, \tag{2}$$

where N_1, N_2, N_3 are shape functions. The values of these shape functions are defined by

$$N_i=\frac{1}{2\triangle^e}(a_i+b_ix+c_iy)(i=1,2,3), \tag{3}$$

where $\triangle^e$ is the area of the element Ω^e and the coefficients a_i, b_i, c_i are calculated by the coordinates of the element Ω^e:

$$\begin{aligned} &a_1=x_2y_3-x_3y_2, b_1=y_2-y_3, c_1=x_3-x_2,\\ &a_2=x_3y_1-x_1y_3, b_2=y_3-y_1, c_2=x_1-x_3,\\ &a_3=x_1y_2-x_2y_1, b_3=y_1-y_2, c_3=x_2-x_1. \end{aligned} \tag{4}$$

Using the Galerkin approach, the governing equation of the element Ω^e can be obtained by the integral of the product of the residual and the weighted function. As a weighted residual approach, the Galerkin approach requires the integral to be zero. Considering the natural boundary conditions, the equation of the element Ω^e can be written as:

$$\begin{aligned} &\iint_{\Omega^e}\nu^e(\frac{\partial \mathbf{A}^e}{\partial x}\frac{\partial \mathbf{W}^e}{\partial x}+\frac{\partial \mathbf{A}^e}{\partial y}\frac{\partial \mathbf{W}^e}{\partial y})dxdy\\ &+\iint_{\Omega^e}\sigma^e\frac{\partial \mathbf{A}^e}{\partial t}\mathbf{W}^e dxdy=\iint_{\Omega^e}\mathbf{J}_z^e\mathbf{W}^e dxdy, \end{aligned} \tag{5}$$

where $\mathbf{W}^e$ is the weighting function. Combining the functions (2) and (5) and setting the weighting function to be the same as the shape function, the magnetic vector potential equations can be written as:

$$\begin{aligned} &\frac{\nu^e}{4\Delta^e}\begin{bmatrix}k_{11}&k_{12}&k_{13}\\k_{21}&k_{22}&k_{23}\\k_{31}&k_{32}&k_{33}\end{bmatrix}\begin{bmatrix}A_1^e\\A_2^e\\A_3^e\end{bmatrix}\\ &+\frac{\sigma^e\Delta^e}{12}\begin{bmatrix}2&1&1\\1&2&1\\1&1&2\end{bmatrix}\begin{bmatrix}\frac{\partial A_1^e}{\partial t}\\\frac{\partial A_2^e}{\partial t}\\\frac{\partial A_3^e}{\partial t}\end{bmatrix}=\frac{J_z^e\Delta^e}{3}\begin{bmatrix}1\\1\\1\end{bmatrix}, \end{aligned} \tag{6}$$

where $k_{ij}=b_ib_j+c_ic_j(i=1,2,3;j=1,2,3)$, the second term in the left hand is related to the eddy current.

Assembling the equations (6) for all the elements the global nonlinear system given as:

$$\mathbf{KA}+\mathbf{M}\frac{\partial \mathbf{A}}{\partial t}=\mathbf{Q} \tag{7}$$

is formed, where $\mathbf{A}=[A_1A_2\cdots A_n]^T$ is the matrix of the magnetic vector potentials of all nodes; n is the number of the nodes; $\mathbf{K}$ is the coefficient matrix, and its entry $K_{(ij)}$ is the sum of the coefficients of the same node in each finite element; $\mathbf{M}$ is the coefficient matrix about the σ; and $\mathbf{Q}$ is the coefficient matrix about the J_z.

The nonlinear equation set (7) can be solved by the Newton-Raphson method, but this method is inefficient, which requires the solution of a linear equation set in each iteration. Furthermore, the methods to solve the linear equation set, such as Gaussian Elimination, have high computational complexity when the model order is high.

B. Proper Orthogonal Decomposition Based MOR

Reducing the model order is an effective method to reduce the computational time of the (7). By the POD method, a high dimensional data set can be represented by vectors with a lower number of data projection, as expressed by the following equation:

$$\mathbf{A}=\mathbf{\Psi}\mathbf{A}_r, \tag{8}$$

where $\mathbf{\Psi}$ is the projection operator; $\mathbf{A}$ is the original vector of size n and $\mathbf{A}_r$ is the new vector of size r ($r << n$).

To obtain the $\mathbf{\Psi}$, some snapshots need to be prepared first. These snapshots are obtained by solving the original equations (7) for the first N time steps, and they can form a snapshots matrix $\mathbf{A}_s$ as the following equation:

$$\mathbf{A}_s=\left[\mathbf{A}^1,\mathbf{A}^2,\mathbf{A}^3...\mathbf{A}^N\right], \tag{9}$$

where $\mathbf{A}^N$ is the Nth prepared snapshots.

To obtain the projection operator, singular value decomposition (SVD) is applied to $\mathbf{A}_s$, and $\mathbf{A}_s$ is decomposed into three matrices [33]:

$$\mathbf{A}_s=\mathbf{U\Sigma V}^T=\sum_{i=0}^{N}\sigma_i\mathbf{u}_i\mathbf{v}_i^T, \tag{10}$$

where $\mathbf{U}$ and $\mathbf{V}$ are the orthogonal matrices. $\mathbf{\Sigma}$ is the diagonal matrix of the singular values. $\mathbf{u}_i$ and $\mathbf{v}_i$ are the eigenvectors of the $\mathbf{A}_s\mathbf{A}_s^T$ and $\mathbf{A}_s^T\mathbf{A}_s$. σ_i is the square root of the eigenvalues of $\mathbf{A}_s\mathbf{A}_s^T$ and σ_i is listed in the declining order in $\mathbf{\Sigma}$. The columns of $\mathbf{U}$ can be the orthonormal basis of the space and the σ_i implies the degree of importance of these basis. The larger σ_i implies to the more important basis. To reduce the order of (7), the first r columns of $\mathbf{U}$ are selected and the projection operator can be defined by

$$\mathbf{\Psi}=[\mathbf{u}_1,\mathbf{u}_2,...\mathbf{u}_r]. \tag{11}$$

The low-order approximation of the equation set (7) can be obtained based on the $\mathbf{\Psi}$ as:

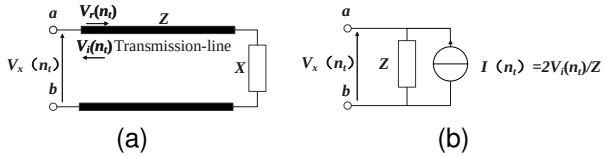

Fig. 2. (a) TLM section, and (b) its Norton equivalent circuit.

$$\mathbf{K}_r\mathbf{A}_r + \mathbf{M}_r\frac{\partial \mathbf{A}_r}{\partial t} = \mathbf{Q}_r, \tag{12}$$

where $\mathbf{A}_r = \mathbf{\Psi}^T\mathbf{A}$, $\mathbf{K}_r = \mathbf{\Psi}^T\mathbf{K}\mathbf{\Psi}$, $\mathbf{M}_r = \mathbf{\Psi}^T\mathbf{M}\mathbf{\Psi}$ and $\mathbf{Q}_r = \mathbf{\Psi}^T\mathbf{Q}$.

The order of the new equation set (12) is only r and may appear easy to solve. However, in the electromagnetic finite element model, as shown in (7), the $\mathbf{K}$ is obtained by the nonlinear magnetic permeability calculated based on the magnetic flux density B. It is necessary to update the $\mathbf{K}_r$ by the $\mathbf{K}$ in every time-step when solving the equation set (12). In particular, the Jacobian matrix is difficult to be obtained when solving the above equation set (12) by the Newton-Raphson method because the values in the $\mathbf{K}_r$ lose their original relationship with the FE nodes. Obtaining $\mathbf{K}_r$ and the Jacobian matrix will cost excessive time when solving the reduced-order model. Here the TLM method is used to solve this problem.

C. Proposed Combination of the POD and the TLM (POD + TLM)

The TLM technique is used to decouple the nonlinear components from the linear network and is suitable for parallel solution. This technique can effectively improve computational efficiency. The TLM calculation is based on the transmitting voltage pulses along the transmission lines. The final result is obtained after many times TLM iterations. First, transmission lines are added to the original circuit. In each time-step, pulses are injected from each nonlinear external element to the linear network, and the reflected pulses of the linear network can be computed. Then the newly injected pulses from each nonlinear external element can be calculated separately. After several iterations, the result finally converges to the original circuit result. Fig. 2 is a schematic for one of the nonlinear resistors in the whole network. Fig. 2 (a) presents a transmission line section, and Fig. 2 (b) is the Norton equivalent circuit which contains characteristic resistance and current source for this TLM section. In the iteration n_t, the node voltage $V_x(n_t)$ between two nodes consist of the incident pulses $V_i(n_t)$ and reflected pulses $V_r(n_t)$ [30]:

$$V_x(n_t) = V_i(n_t) + V_r(n_t), \tag{13}$$

where X is the nonlinear element in Fig. 2. The current (I)-voltage (U) law of X can be described as $I = G(U)$. According to the transmission line method, the following equation must be established at every step, so the next incident pulse from the nonlinear element can be calculated by:

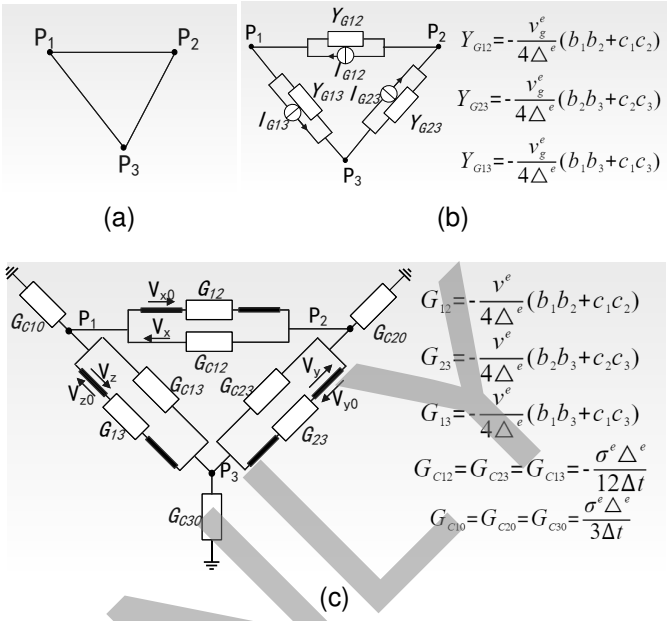

Fig. 3. Equivalent electrical network of finite element based on the TLM: (a) finite element; (b) Norton equivalent circuit of TLM sections; (c) equivalent circuit of finite element.

$$\frac{V_r(n_t) - V_i(n_t+1)}{Z} = G(V_r(n_t) + V_i(n_t+1)), \tag{14}$$

where Z is the characteristic impedance of the transmission line, and then the $V_i(n_t+1)$ and Z will be used to replace the nonlinear element in the calculation of the linear network to get the $V_x(n_t+1)$. This means that a network containing n nonlinear elements can be solved in terms of n separated equations rather than n connected nonlinear equations. Thus, all elements are decoupled from the network. The Backward Euler discretization method is used to solve (6) and obtain the following equation:

$$\begin{aligned}
&\frac{\nu^e}{4\Delta^e}\begin{bmatrix} k_{11} & k_{12} & k_{13} \\ k_{21} & k_{22} & k_{23} \\ k_{31} & k_{32} & k_{33} \end{bmatrix}\begin{bmatrix} A_1^e(t+\Delta t) \\ A_2^e(t+\Delta t) \\ A_3^e(t+\Delta t) \end{bmatrix} \\
&\quad + \frac{\sigma^e\Delta^e}{12\Delta t}\begin{bmatrix} 2 & 1 & 1 \\ 1 & 2 & 1 \\ 1 & 1 & 2 \end{bmatrix}\begin{bmatrix} A_1^e(t+\Delta t) \\ A_2^e(t+\Delta t) \\ A_3^e(t+\Delta t) \end{bmatrix} = \\
&\frac{J_z^e(t+\Delta t)\Delta^e}{3}\begin{bmatrix} 1 \\ 1 \\ 1 \end{bmatrix} + \frac{\sigma^e\Delta^e}{12\Delta t}\begin{bmatrix} 2 & 1 & 1 \\ 1 & 2 & 1 \\ 1 & 1 & 2 \end{bmatrix}\begin{bmatrix} A_1^e(t) \\ A_2^e(t) \\ A_3^e(t) \end{bmatrix}.
\end{aligned} \tag{15}$$

Because of the similarity between the finite element matrix and the nodal admittance matrix of an electrical network, the TLM method has been successfully used in the FEM. The elemental equation (15) of FEM is equivalent to the electrical network as shown in Fig. 3. Fig. 3, which is a schematic for one of all elements in the whole network and every element can be separated similarly.

In Fig. 3 (c) the nonlinear parts are the G_{12}, the G_{13} and the G_{23}. These parts are separated by the transmission-lines. The

This article has been accepted for publication in IEEE Open Access Journal of Power and Energy. This is the author's version which has not been fully edited and content may change prior to final publication. Citation information: DOI 10.1109/OAJPE.2022.3197431

reflected pulses in Fig. 3 are denoted by V_{x0}, V_{y0} , and V_{z0} and the incident pulses are denoted by V_x, V_y , and V_z. The Norton equivalent circuit of TLM sections are shown in Fig. 3 (b). The v^e is the accuracy magnetic reluctivity, and the v_g^e is the guess magnetic reluctivity used to obtain the characteristic admittance Y. Select the characteristic admittance Y which is close to the values of the nonlinear admittance G can effectively reduce the number of TLM iterations [14]. In each time-step, each nonlinear element can be solved by the following equation individually according to the following equation:

$$\begin{aligned} G_{12}(V_{x0}(n_t)+V_x(n_t+1)) &= Y_{G12}(V_{x0}(n_t)-V_x(n_t+1)) \\ G_{13}(V_{y0}(n_t)+V_y(n_t+1)) &= Y_{G12}(V_{y0}(n_t)-V_y(n_t+1)) \\ G_{23}(V_{z0}(n_t)+V_z(n_t+1)) &= Y_{G23}(V_{z0}(n_t)-V_z(n_t+1)). \end{aligned} \tag{16}$$

Based on the TLM method, the linear portion and the nonlinear portion are separated, and all the nonlinear elements can be solved in parallel that means many three order nonlinear equations will be solved simultaneously, which only needs little execution time. When solving the whole network only the characteristic admittances are used. That means the equation set (7) can be solved without changing the $\mathbf{K}$ and $\mathbf{M}$. The equation (7) is changed into:

$$\mathbf{SA} = \mathbf{Q}, \tag{17}$$

where $\mathbf{S} = \mathbf{K} + \mathbf{M}\frac{\partial}{\partial t}$. $\mathbf{S}$ is not changed when solving this equation. But this high order linear portion will be time-consuming and would need too much hardware resource, so we use POD to reduce the latency and resource of the linear portion, as follows:

$$\mathbf{S}_r\mathbf{A}_r = \mathbf{Q}_r, \tag{18}$$

where $\mathbf{S}_r = \mathbf{\Psi}^T\mathbf{S}\mathbf{\Psi}$. The $\mathbf{S}_r$ in this equation set also does not need to be changed; hence this matrix can be obtained before the simulation. The nonlinear element only influences the whole network by the equivalent current source, which is incident in $\mathbf{Q}_r$. The equation set (18) becomes a low-order linear model, which can be solved by Gaussian Elimination or other methods. The whole process of solving the electromagnetic field based on the proposed POD + TLM method is shown in flow chart given in Fig. 4. Although in each iteration, it takes some time to calculate the $\mathbf{A}$ and $\mathbf{Q}_r$ by (8) for obtaining the node voltages and the current sources for the TLM, the proposed method still saves a lot of time by replacing the high-order model with a low-order model. The TLM often requires more iterations to converge than the Newton-Raphson algorithm, especially when the difference between the characteristic admittances obtained from the TLM and the actual nonlinear admittances is significant. Changing the value of the characteristic admittance at each iteration is a solution to reduce the iterations by decreasing the difference between the admittances of TLM and the actual model. However, changing the characteristic admittance means changing the $\mathbf{K}$ and $\mathbf{S}$, re-assembling the matrices and reducing their order that wastes a lot of time and hardware resources. To solve this

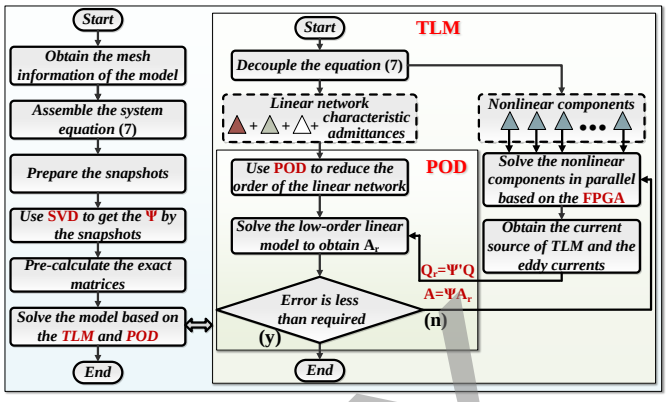

Fig. 4. Flowchart of the proposed POD + TLM method.

problem, we pre-calculate the exact matrices $\mathbf{S}$ and $\mathbf{S_r}$ by the equation in Fig. 3 (c) based on the already obtained snapshot. This approach can reduce iterations to improve computational efficiency effectively. The proposed method can use more pre-calculated matrices than the previous TLM method because the low-order matrices take up fewer resources.

III. Field-Circuit Coupling for Electromagnetic Transient Simulation

The above method facilitates the simulation of the transformer excited by the known coil currents. However, transformers are often excited by the external circuit. A field-circuit coupling method is needed in the simulation of the three-phase transformer working with the external circuit. The indirect coupling method is used in this work. This method separately considers the FE model equations and the external circuit equations. It is a common method which has been used in many papers such as [34] and can ensure the enough accuracy of the results. In this paper, the low-order model is used to realize the indirect coupling method. When the transformer is excited by the external circuit, the electromotive force (EMF) of the coils direct influences the circuit. Based on the Kirchhoff's voltage circuit law the following equation about the voltages of the circuit can be obtained:

$$F(\mathbf{I}) = \mathbf{V_{ex}} + \mathbf{V_{coil}} = 0, \tag{19}$$

where $\mathbf{V_{ex}}$ is the voltages of the external circuit, $\mathbf{V_{coil}}$ is the voltages of the coil and can be got by the EMF. $\mathbf{V_{ex}}$ and $\mathbf{V_{coil}}$ are the vectors that depend on $\mathbf{I}$ which is the matrix of the coils' currents. Each entry of $\mathbf{V_{ex}}$ is the function of the current only on its branch circuit, and each entry of $\mathbf{V_{coil}}$ is influenced by all the currents because of the electromagnetic conversion in the transformer. For the three-phase transformer in this work, all the above vectors are 6×1 vectors.

Solving (19) by Newton-Raphson method can realize the field-circuit coupling, for which the Jacobian matrix is needed. It is important to get the relationship between the voltages and currents. The relationship between $\mathbf{V_{ex}}$ and $\mathbf{I}$ can be obtained according to the performance of the circuit components such as resistance, capacitance, and inductance. According to (1), magnetic vector potentials are related to the currents. Faraday's

law states that the EMF is generated on the conductive loop when the magnetic flux through the surface enclosed by the loop varies in time, and the magnetic flux density can be calculated by the magnetic vector potentials. Thus, the relationship between magnetic vector potentials and EMF can be obtained as

$$V^e = \sum_{i=1}^{3} \frac{\partial A_i}{\partial t} \oint_{\Gamma^e} (N_w \cdot N_i \cdot \hat{n}) dl = \mathbf{A_w^e} \cdot \frac{\partial \mathbf{A^e}}{\partial t}, \qquad (20)$$

where V^e is the EMF, N_w is the coil turns, N_i is the interpolation functions and $\hat{n}$ is the unit vector of the wire direction. Based on this equation, $\mathbf{A_w^e}$ is used as the weight of the $\mathbf{A^e}$ at each node in this element to get the V^e. $\mathbf{A_w^e}$ and $\mathbf{A^e}$ can also use the low-order model in this part. Each coil EMF of the transformer can be obtained by the sum of the EMF of all small elements in the same coil. According to equations (20) and (6) the relationship between the $\mathbf{V_{coil}}$ and $\mathbf{I}$ is obtained. Then the equation (19) with the unknowns $\mathbf{I}$ can be solved by the Newton-Raphson method.

IV. Real-Time Hardware Emulation on FPGA

The electromagnetic field simulation and field-circuit coupling simulation processes involve operations such as matrix synthesis, matrix addition, that can be done in parallel. FPGAs are well suited for parallel implementation due to the unroll and pipeline operations. Developers can easily use the optimization directives to change their C or C++ programs into the hardware IP blocks by the high-level synthesis (HLS) and realize the unroll and pipeline in their programs. In this work the optimized hardware blocks are deployed on the Xilinx® Virtex® UltraScale+ HBM VCU128-ES1 board with the XCVU37P-fsvh2892-2L-e FPGA.

The generated hardware blocks can be divided into two groups. One group is focused on obtaining the magnetic vector potentials by solving (7) based on the POD and the TLM, and this group is called FEM Solver Group. The other group is used to solve (19) by the Newton-Raphson method based on the magnetic vector potentials obtained by the FEM group, and this group is called the field-circuit coupling group.

The blocks in the FEM Solver Group are presented as the following, and the hardware architecture of these blocks is shown in Fig. 5 (only the most important variables are given in the figure):

1) *External current*: The $\mathbf{Q}$ in (7) are influenced by three parts: coil current density from the external circuit I_{coil}, the coil source current density caused by the TLM technique, and the eddy current density. This block is used to obtain the external current density. With the external current obtained from the external circuit the external current density is obtained by this block. This block uses the loop unroll operations to get the external current density on each node in parallel.
2) *Eddy current*: The eddy current density is related to the magnetic vector potentials of the previous time-step, so the magnetic vector potentials is the input of this block.

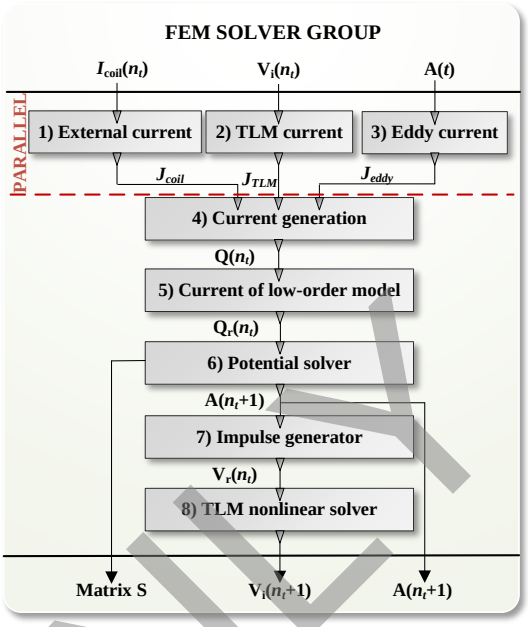

Fig. 5. Hardware architecture for FEM solver based on the proposed POD + TLM method.

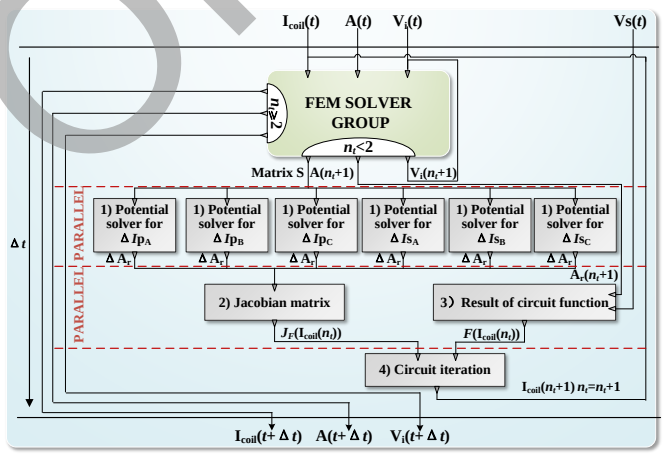

Fig. 6. Hardware architecture for field-circuit coupling based on Newton-Raphson iteration.

The pipeline operations are used here to reduce the time for the matrix-vector multiplication in this block.

3) *TLM current*: The TLM current density can be calculated by the incident pulses in each small element. This block obtains the incident pulses from the TLM nonlinear solver block as inputs and calculates the current injected to each node. The pipeline operations are used to calculate the current of different nodes.
4) *Current Generator*: This block receives all of the above three current densities as the inputs and accumulates the current density of the same node to calculate the $\mathbf{Q}$ of (7). All the nodes is calculated in parallel by loop unroll.
5) *Current of low-order model*: This block is used to obtain the $\mathbf{Q}_r$. The input of this block is the $\mathbf{Q}$. The $\mathbf{\Psi}$ has already been prepared. The $\mathbf{Q}_r$ can be calculated by the product of the vector $\mathbf{Q}$ and the matrix $\mathbf{\Psi}$. In this block,

the pipeline operations are used to improve the computational efficiency of the matrix-vector multiplication.

6) *Potential solver*: This block is used to get the magnetic vector potentials of the low-order model by solving (18) and then get the magnetic vector potentials of the high-order model based on the equation (8). The input of this block is obtained by the current of low-order model block. The order of the equations which need to solve is low so that the latency of this block is quite low.
7) *Impulse Generator*: After obtaining the potential of each node, the reflected pulses in the TLM method are obtained by this block based on (13). The reflected pulses can be calculated in parallel by loop unroll operations.
8) *TLM nonlinear solver*: When using the TLM, the incident pulses of each small nonlinear element need to be calculated to get the TLM current. This block is used to obtain the incident pulses by solving the 3×3 nonlinear matrix equation (16). The Newton-Raphson method is used to solve each small nonlinear element in parallel.

The hardware blocks in the field-circuit coupling group are presented as the following and the hardware architecture is shown in Fig. 6:

1) *Potential solver for* ΔI: This block is used to get the relationship between $\mathbf{A}$ and every coil current. Because the ΔI is small this block uses the same $\mathbf{S}$ as used in the FEM solver group. For different ΔI the increment of current density $\Delta \mathbf{Q}$ can be calculated independently, and it will not change over time. By solving the low-order equation $\mathbf{S_r} \times \Delta \mathbf{A_r} = \Delta \mathbf{Q_r}$, we can get $\Delta \mathbf{A_r}$. Here the low-order parameter is output. Because there are six coils, six of these blocks will work in parallel.
2) *Jacobian matrix*: This block is used to obtain the Jacobian matrix of (18). The input of this block is the $\Delta \mathbf{A_r}$ of each coil current. The $\frac{\partial \mathbf{V_{coil}}}{\partial \mathbf{I}}$ can be calculated by (20). Here we can use the low-order parameter. The $\frac{\partial \mathbf{V_{ex}}}{\partial \mathbf{I}}$ is got based on the performance of external circuits. The Jacobian matrix is obtained by combining the above two parts.
3) *Result of circuit function*: This block gets the magnetic vector potentials at this iteration from the FEM solved group. Based on (20), the $\mathbf{V_{coil}}$ can be calculated. Here we can also use the low-order parameters, and the $\mathbf{V_{ex}}$ can be obtained by the performance of external circuits. Then the result of (19) at this iteration is obtained.
4) *Circuit iteration*: In this block, a sixth order equation set will be solved by the Gaussian Elimination method to get the $\Delta \mathbf{I}$, based on Jacobian matrix and the result of the function (19). Finally, the next $\mathbf{I}$ will be obtained.

The hardware resources occupied by these blocks and the latency of each block are shown in Table I.

TABLE I
HARDWARE RESOURCE UTILIZATION AND TIMING REPORT

FPGA Device	Hardware Block	Resource Utilization				Latency (clock cycles)
		BRAM	DSP	FF	LUT	
Xilinx Virtex UltraScale+ xcvu37p-fsvh2892-2L-e	External current	0	128	9685	9668	5
	TLM current	0	41	70965	119984	616
	Eddy current	0	43	42686	102223	401
	Current Generator	0	770	80469	98587	3
	Current of the low-order model	0	1973	180505	121797	40
	Potential solver	16	78	12775	11067	487
	Impulse Generator	0	24	3613	11413	112
	TLM nonlinear solver	76	4123	677572	407419	1185
	$6 \times$ Potential solver for ΔI	0	468	76074	62910	91
	Jacobian matrix	3	90	12137	9257	386
	Result of circuit function	3	78	7812	6816	192
	Circuit iteration	24	25	7841	11191	335
	Total	3%	86%	45%	75%	4308

V. CASE STUDIES AND RESULTS

A. Setup for Case Studies

A three-phase power transformer rated at 40kV/200kV was used as an example to verify the proposed POD + TLM method in this work. The geometry and mesh of this transformer are shown in Fig. 1. The mesh of this transformer has 385 nodes and 728 finite elements. The elements can be divided into four types. The transformer core elements are nonlinear while the others are linear. The nonlinear material permeability of the transformer core elements depends on the magnetic field density and can be described by the following equation:

$$H = \begin{cases} 800\text{BAT/m} & \text{if } 0 < B < 0.6, \\ 800\text{B} + 10^5(\text{B} - 0.6)^3\text{AT/m} & \text{if } B > 0.6. \end{cases} \quad (21)$$

There are two case studies presented in this work: external current excitation and external circuit excitation. The current excitation (Case Study I) show the accuracy of the proposed MOR method, with the focus being on the result accuracy of each node. The external circuit excitation (Case Study II) further verifies the accuracy of the field-circuit coupling; here the focus is on the accuracy of the current and the voltage of each coil. The hardware emulation of the above case studies is performed on Xilinx® Virtex® UltraScale+ HBM VCU128-ES1 board. The main hardware resources of the Xilinx® XCVU37P FPGA are as follows: 4032 BRAMs, 9024 DSP48E slices, 2607360 flip-flops, and 1303680 look-up table. Compared with the case study in the reference [12] and [14], for the similar transformer model, two FPGAs are used in these papers to solve the full order model but one FPGA is enough for the low order model in this paper. The full order model is also difficult to further apply to the 3D and rotating machine geometries. The proposed method is very useful to reduce the resource. The simulation has been done again by the commonly used FEM software Comsol® to obtain relatively accurate results for comparison.

For Case Study I, the current source of each phase can be written as $I_A(t) = 500sin(120\pi t)$ A, $I_B(t) = 500sin(120\pi t - 2/3\pi)$ A, and $I_C(t) = 500sin(120\pi t + 2/3\pi)$ A respectively. The results such as magnetic vector potential of each node from the low-order model and Comsol® are

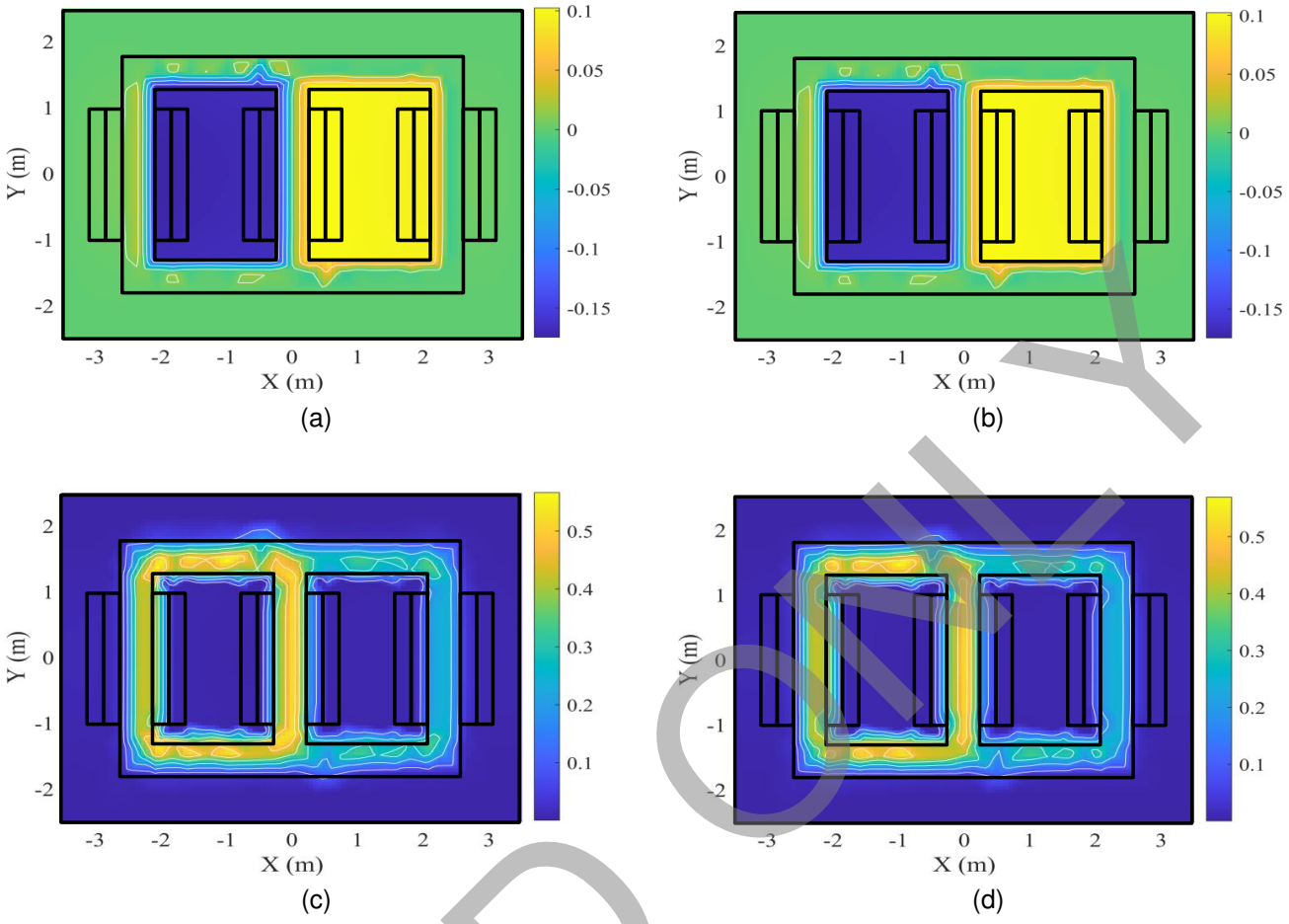

Fig. 7. Magnetic vector potential distributions and magnetic flux density distributions at time $t = 5$ ms. Magnetic vector potential distribution from real-time emulation (a), and from Comsol® (b). Magnetic flux density from real-time emulation (c), and from Comsol® (d).

compared. The error of these nodes is used to verify the accuracy in this case study. The order of the model is also considered to find a balance between the calculation efficiency, resource, and accuracy.

For Case Study II, the external circuits connected to the transformer are shwon in Fig. 1 and the three phases use the same circuit. The voltage of each phase can be written as $V_A = 40\sqrt{2}sin(120\pi t)$ kV, $V_B = 40\sqrt{2}sin(120\pi t - 2/3\pi)$ kV, $V_C = 40\sqrt{2}sin(120\pi t + 2/3\pi)$ kV respectively. The switch S_1 is turned on at $t = 0$ s and the S_2 is turned on at $t = 50$ ms. The third and fifth harmonics of 6.67kV and 4kV respectively are injected at $t = 100$ ms. The currents and voltages for each coil of the transformer are compared in this case study.

B. Results and Validation of Case Study I

In Case Study I, the transformer is excited by the ac currents directly. The accuracy of the proposed MOR mehod is easy to be observed in this case study by ignoring the external circuit. All the hardware blocks of the FEM solved group were used in this case study.

The model order is set to 16 at the beginning to verify the accuracy. Using the 100 MHz hardware clocks, the calculation

TABLE II
HARDWARE RESOURCE CONSUMPTION FOR DIFFERENT MODEL ORDERS

Hardware Block	Order	Resource Utilization				Latency (clock cycles)
		BRAM	DSP	FF	LUT	
Current of low-order model	8	0 (0%)	1937 (21.5%)	180502 (6.9%)	120345 (9.2%)	32
	16	0 (0%)	1937 (21.5%)	180505 (6.9%)	121797 (9.3%)	40
	32	363 (9.0%)	1973 (21.9%)	168892 (6.5%)	118893 (9.1%)	56
Potential solver	8	8 (0.2%)	38 (0.4%)	6469 (0.2%)	6523 (0.5%)	467
	16	16 (0.4%)	78 (0.9%)	12775 (0.5%)	11067 (0.8%)	487
	32	384 (9.5%)	316 (3.5%)	925679 (35.5%)	25149 (1.9%)	524
Potential solver for ΔI	8	0 (0%)	38 (0.4%)	6375 (0.2%)	6181 (0.5%)	73
	16	0 (0%)	78 (0.9%)	12679 (0.5%)	10485 (0.8%)	91
	32	352 (8.7%)	158 (1.8%)	12975 (0.5%)	15573 (1.2%)	125

This article has been accepted for publication in IEEE Open Access Journal of Power and Energy. This is the author's version which has not been fully edited and content may change prior to final publication. Citation information: DOI 10.1109/OAJPE.2022.3197431

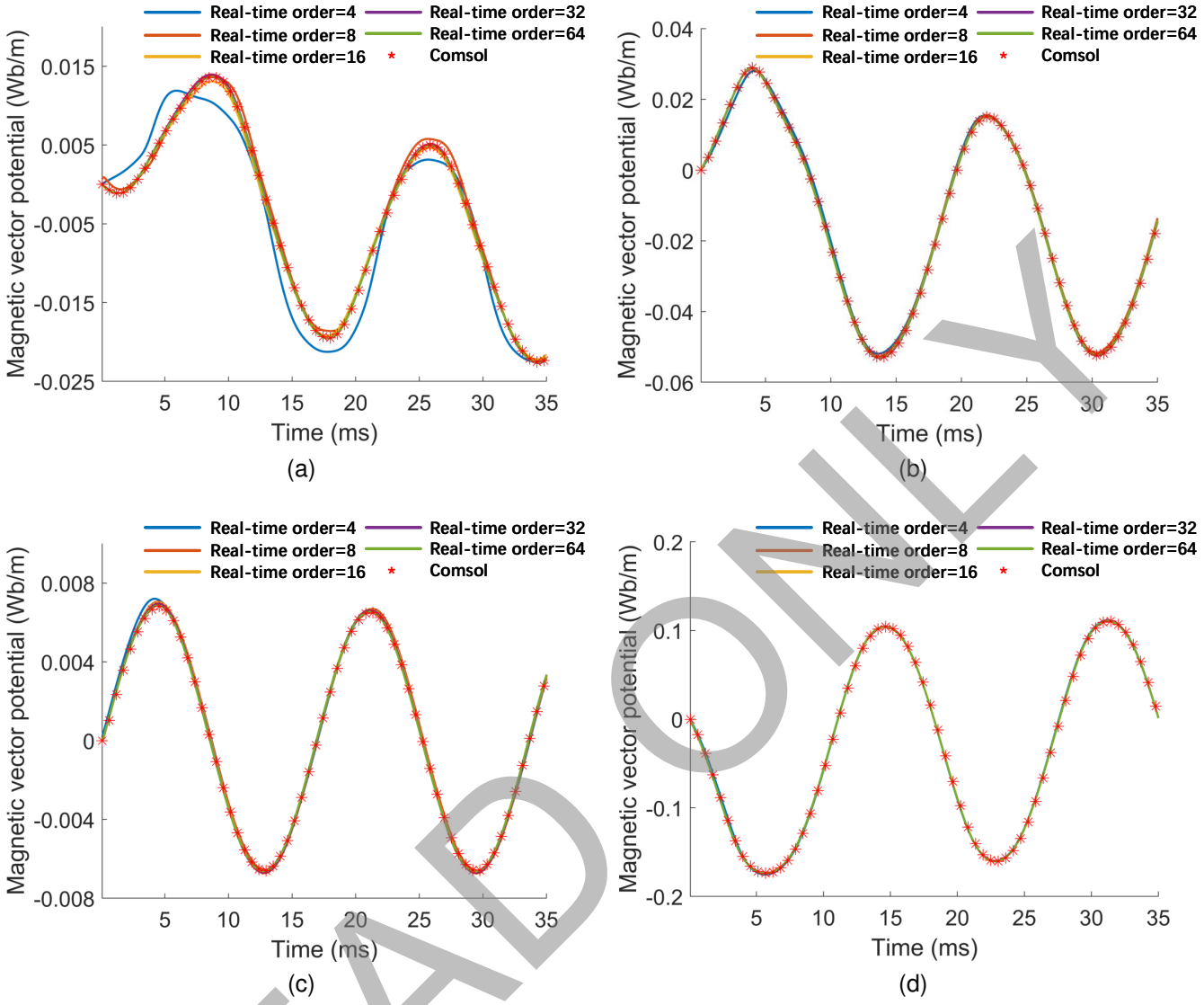

Fig. 8. Comparison for the magnetic vector potential at probes from Comsol® and real-time emulation: Magnetic vector potential at probe point in Fig. 1: Probe A (a), Probe B (b), Probe C (c), Probe D (d).

time for one TLM iteration is about (616 + 3 + 40 + 487 +112 + 1185) ÷ 100 = 24.43 μs. The time-step in this case study is set as $\Delta t = 70$ μs so that two TLM iterations can be performed in one time-step. The time-step is small enough to guarantee accuracy with few TLM iterations. The execution time is less than the time-step so that the real-time constraint can be realized. The magnetic vector potentials and magnetic flux density are chosen as typical results to compare between the proposed method and the Comsol®. The distributions of these results are shown in Fig. 7, and the error of each node is low. To clearly describe the error, four typical probe nodes are chosen, which are shown in Fig. 1. Probe A and Probe B belong to the nonlinear region. Probe C belongs to the linear coil region. Probe D belongs to the linear air region. The magnetic vector potentials of these four nodes is shown in Fig. 8. Since the model order also influences the results of the real-time simulation, here the order of the model is set as 4, 8, 16, 32, and 64. The results are also shown in Fig. 8. When the order is more than four, the results obtained by real-time simulation are basically consistent with those obtained by Comsol®. Thus, setting the order of the nodes to 8 or more is enough, and the accuracy will improve with the order improved. The model order not only influences the accuracy but also influences the latency and resource. It is helpful to minimize latency and resources while maintaining accuracy. Here the order of models is set as 8, 16, 32 to be further compared. For the hardware blocks: Current of the low-order model, Potential solver, and Potential solver for ΔI, the latency and resource are shown in Table II and the percentage of hardware block's resources in the FPGA are also shown in the parentheses. Considering that the coupling simulation of the transformer requires using the Potential Solver for ΔI many times, the latency and resources need to be low; therefore, setting the model order to 16 is enough for the accuracy, resource, and latency in the following case study.

This article has been accepted for publication in IEEE Open Access Journal of Power and Energy. This is the author's version which has not been fully edited and content may change prior to final publication. Citation information: DOI 10.1109/OAJPE.2022.3197431

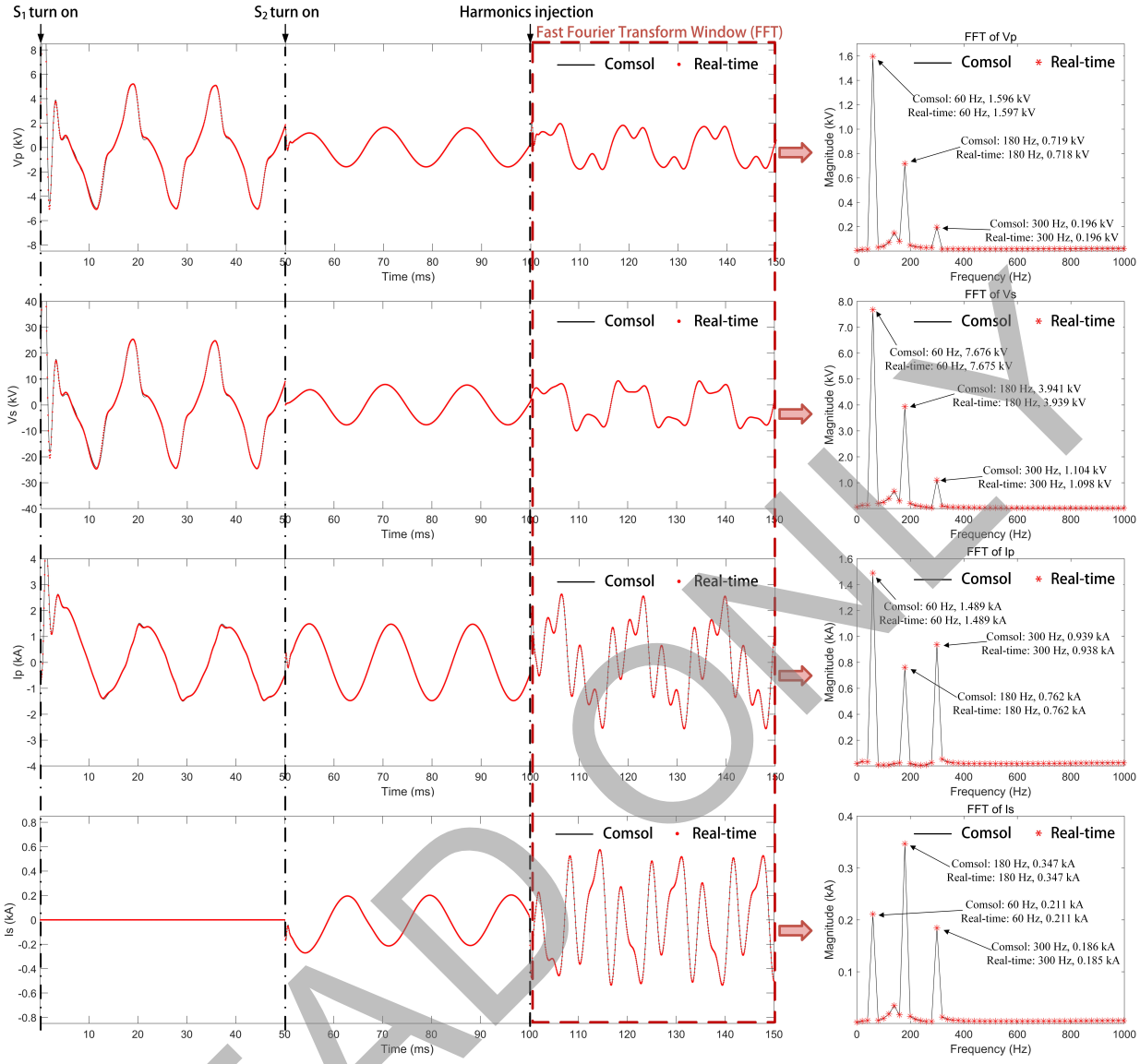

Fig. 9. Real-time emulation results from the proposed POD + TLM method and the comparison with Comsol® results for Case Study II.

C. Results and Validation of Case Study II

For Case Study II, the calculation time for one time step is about $2 \times (616 + 3 + 40 + 487 + 112 + 1185 + 386 + 335 + 91) \div 100 = 65.1\ \mu$s. The time-step in this case study is set as $\Delta t = 70\ \mu$s and two circuit iterations are solved in one time-step. This time-step implies that a 14280 sampling frequency and harmonics in frequency as high as 7.14 kHz could be captured. It is enough for the studied power system. The power electronic systems will be study in our future work. The results of this case study prove the accuracy of the real-time coupling simulation of the proposed method.

During the process of coupling simulation, the voltage on the primary side V_p, the current on the primary side I_p, the voltage on the secondary side V_s, and the current on the secondary side I_s received attention. In this part the results of the A-phase from the real-time simulation and the Comsol® are compared (Fig. 9). The results are also analyzed in the frequency-domain in Fig. 9. As can be seen from these figures, the results from the real-time simulation are quite close to those from off-line Comsol®. Compared the results of the proposed method and the Comsol®, the mean absolute relative error is within 6% which meets the requirements of practical use.

VI. Conclusion

For real-time electromagnetic finite element transient simulation, this paper proposed a model order reduction method based on the combination of the POD method and the TLM based solution scheme. Since the original POD methods have limitations at solving nonlinear problems, the proposed method uses the TLM technique to decouple nonlinear elements from the linear network, and the POD method is only used to reduce the order of the linear domain model to improve computational efficiency. The nonlinear elements can be calculated in parallel, improving the computational efficiency. The FPGA is used as a hardware platform to realize the above method based

on unrolling and pipelining schemes to achieve a high degree of parallelism in the realization of real-time emulation of a three-phase transformer. The results from the proposed method were compared with the commercial FEM software, Comsol®. The comparison results show that the proposed method has high computational efficiency and excellent accuracy. Based on multiple interconnected FPGA boards with higher resource count, the accuracy and efficiency can be further improved by increasing the order of the finite element model. After separating nonlinear elements from the 3D finite element model by the 3D TLM method and then the POD can be used to solve the 3D case. Therefore, in the future the proposed method will be also helpful to solving nonlinear problems with a larger number of nodes and for 3D geometries.

APPENDIX

Transformer parameters: the size of the outer rectangle is 3.6 m $\times$ 5.2 m, the two small inner rectangles are both 2.6 m $\times$ 1.85 m, the width of the transformer core is 0.5 m, and the size of the coil is 0.25 m $\times$ 2 m. The number of primary side coil turns is 40 and the number of secondary side coil turns is 200. The σ^e is 1000. The parameters of the external circuit are: $R_1 = R_2 = 10\ \Omega$, $L_1 = L_2 = 46$ mH, and $C_1 = C_2 = 93$ μF.

REFERENCES

[1] *Electrical Transmission and Distribution Reference Book*. Westinghouse Electric Corporation; 4th edition, 1964.

[2] J. A. Martinez and B. A. Mork, "Transformer modeling for low-and mid-frequency transients-a review," *IEEE Trans. on Power Delivery*, vol. 20, no. 2, pp. 1625–1632, April 2005.

[3] B. A. Mork, F. Gonzalez, D. Ishchenko, D. L. Stuehm, and J. Mitra, "Hybrid transformer model for transient simulation-part I: Development and parameters," *IEEE Trans. Power Del.*, vol. 22, no. 1, pp. 248–255, 2006.

[4] J. R. Brauer and J. J. Ruehl, "Finite element modeling of power electronic circuits containing switches attached to saturable magnetic components," *IEEE Trans. Energy Conversion*, vol. 14, no. 3, pp. 589–594, 1999.

[5] A. Taher, S. Sudhoff, and S. Pekarek, "Calculation of a tape-wound transformer leakage inductance using the MEC model," *IEEE Trans. Energy Conversion*, vol. 30, no. 2, pp. 541–549, 2015.

[6] M. Luo, D. Dujic, and J. Allmeling, "Leakage flux modeling of multiwinding transformers for system-level simulations," *IEEE Trans. Power Electron.*, vol. 33, no. 3, pp. 2471–2483, 2017.

[7] N. B. Chagas and T. B. Marchesan, "Analytical calculation of static capacitance for high-frequency inductors and transformers," *IEEE Trans. Power Electron.*, vol. 34, no. 2, pp. 1672–1682, 2018.

[8] S. Mohammadi, M. Mirsalim, and S. Vaez-Zadeh, "Nonlinear modeling of eddy-current couplers," *IEEE Trans. Energy Conversion*, vol. 29, no. 1, pp. 224–231, 2013.

[9] A. Narang and R. H. Brierley, "Topology based magnetic model for steady-state and transient studies for three-phase core type transformers," *IEEE Trans. Power Syst.*, vol. 9, no. 3, pp. 1337–1349, 1994.

[10] V. Dinavahi and N. Lin, *Real-Time Electromagnetic Transient Simulation of AC-DC grids*. Wiley-IEEE Press: New Jersey, 2021.

[11] J. Liu and V. Dinavahi, "Detailed magnetic equivalent circuit based real-time nonlinear power transformer model on FPGA for electromagnetic transient studies," *IEEE Trans. on Industrial Electronics*, vol. 63, no. 2, pp. 1191–1202, Feb. 2016.

[12] Q. Xu, P. Liu, and V. Dinavahi, "Time-stepped finite-element modeling of three-phase transformer for electromagnetic transient emulation on FPGA," *IEEE Open Access Journal of Power and Energy*, vol. 8, pp. 239–247, June 2021.

[13] P. Liu, J. Li, and V. Dinavahi, "Matrix-free nonlinear finite-element solver using transmission-line modeling on GPU," *IEEE Trans. Magn.*, vol. 55, no. 7, pp. 1–5, 2019.

[14] P. Liu and V. Dinavahi, "Real-time finite-element simulation of electromagnetic transients of transformer on FPGA," *IEEE Trans. Power Del.*, vol. 33, no. 4, pp. 1991–2001, 2018.

[15] R. C. Degeneff, M. Gutierrez, S. Salon, D. Burow, and R. Nevins, "Kron's reduction method applied to the time stepping finite element analysis of induction machines," *IEEE Trans. Energy Conversion*, vol. 10, no. 4, pp. 669–674, 1995.

[16] B. Hassard and Y. H. Wan, "Bifurcation formulae derived from center manifold theory," *Journal of Mathematical Analysis and Applications*, vol. 63, no. 1, pp. 297–312, 1978.

[17] N. Sidorov, B. Loginov, A. Sinitsyn, and M. Falaleev, *Lyapunov-Schmidt methods in nonlinear analysis and applications*. Springer Science & Business Media, 2013.

[18] S. L. Ho, Y. Zhao, and W. Fu, "Adaptive discontinuous Galerkin method for transient analysis of eddy current fields in high-speed rotating solid rotors," *IEEE Trans. Magn.*, vol. 50, no. 2, pp. 589–592, 2014.

[19] C. Foias, G. R. Sell, and R. Temam, "Inertial manifolds for nonlinear evolutionary equations," *Journal of differential equations*, vol. 73, no. 2, pp. 309–353, 1988.

[20] B. García-Archilla, J. Novo, and E. S. Titi, "Post-processing the Galerkin method: a novel approach to approximate inertial manifolds," *SIAM journal on numerical analysis*, vol. 35, no. 3, pp. 941–972, 1998.

[21] R. D. Slone, R. Lee, and J.-F. Lee, "Multipoint Galerkin asymptotic waveform evaluation for model order reduction of frequency domain FEM electromagnetic radiation problems," *IEEE Trans. Antennas Propagat.*, vol. 49, no. 10, pp. 1504–1513, 2001.

[22] A. Steindl and H. Troger, "Methods for dimension reduction and their application in nonlinear dynamics," *International Journal of Solids and Structures*, vol. 38, no. 10-13, pp. 2131–2147, 2001.

[23] S. Clenet, T. Henneron, and N. Ida, "Reduction of a finite-element parametric model using adaptive POD methods- application to uncertainty quantification," *IEEE Trans. Magn.*, vol. 52, no. 3, pp. 1–4, 2015.

[24] W. Wang, G. N. Paraschos, and M. N. Vouvakis, "Fast frequency sweep of fem models via the balanced truncation proper orthogonal decomposition," *IEEE Trans. Antennas Propagat.*, vol. 59, no. 11, pp. 4142–4154, 2011.

[25] S. Banerjee, J. V. Cole, and K. F. Jensen, "Nonlinear model reduction strategies for rapid thermal processing systems," *IEEE Trans. Semiconduct. Manufact.*, vol. 11, no. 2, pp. 266–275, 1998.

[26] T. Henneron and S. Clenet, "Model-order reduction of multiple-input non-linear systems based on POD and DEI methods," *IEEE Trans. Magn.*, vol. 51, no. 3, pp. 1–4, 2015.

[27] M. N. Albunni, V. Rischmuller, T. Fritzsche, and B. Lohmann, "Model-order reduction of moving nonlinear electromagnetic devices," *IEEE Trans. Magn.*, vol. 44, no. 7, pp. 1822–1829, 2008.

[28] T. Henneron and S. Clenet, "Model order reduction of non-linear magnetostatic problems based on POD and DEI methods," *IEEE Trans. Magn.*, vol. 50, no. 2, pp. 33–36, 2014.

[29] P. B. Johns and M. O' Brien, "Use of the transmission-line modelling (t.l.m.) method to solve non-linear lumped networks," *Radio and Electronic Engineer*, vol. 50, no. 1.2, pp. 59–70, 1980.

[30] O. Deblecker, J. Lobry, and C. Broche, "Use of transmission-line modelling method in fem for solution of nonlinear eddy-current problems," *IEE Proceedings- Science, Measurement and Technology*, vol. 145, no. 1, pp. 31–38, 1998.

[31] ——, "Novel algorithm based on transmission-line modeling in the finite-element method for nonlinear quasi-static field analysis," *IEEE Trans. Magn.*, vol. 39, no. 1, pp. 529–538, 2003.

[32] O. C. Zienkiewicz, R. L. Taylor, and J. Z. Zhu, *The finite element method: its basis and fundamentals*. Elsevier, 2005.

[33] Y. Liang, H. Lee, S. Lim, W. Lin, K. Lee, and C. Wu, "Proper orthogonal decomposition and its applications-part I: theory," *Journal of Sound and vibration*, vol. 252, no. 3, pp. 527–544, 2002.

[34] J. Li, P. Liu, and V. Dinavahi, "Matrix-free edge-domain decomposition method for massively parallel 3-d finite element simulation with field-circuit coupling," *IEEE Trans. Magn.*, vol. 56, no. 10, pp. 1–9, 2020.

Jiuwei Guo received the B.Sc. and M.Sc. degrees in electrical engineering from Harbin Institute of Technology, China, in 2015 and 2017, respectively. Currently, he is pursuing the Ph.D. degree in the Dept. of Electrical Engineering, Harbin Institute of Technology, Heilongjiang, Harbin, China. From 2021 to 2022, he was study at the University of Alberta, Edmonton, AB, Canada, as a visiting Ph.D. student. His research interests include finite element analysis, real-time simulation, and approximate modeling.

Peng Liu received the B.Sc. and M.Eng. degrees in Electrical Engineering from Harbin Institute of Technology, China, in 2013 and 2015, respectively and the Ph.D. degree in Electrical and Computer Engineering from the University of Alberta, Edmonton, AB, Canada, in 2020. His research interests include computational electromagnetics, high-performance finite element analysis, and parallel and distributed processing.

Venkata Dinavahi (Fellow, IEEE) received the B.Eng. degree in electrical engineering from Visvesvaraya National Institute of Technology (VNIT), Nagpur, India, in 1993, the M.Tech. degree in electrical engineering from the Indian Institute of Technology (IIT) Kanpur, India, in 1996, and the Ph.D. degree in electrical and computer engineering from the University of Toronto, Ontario, Canada, in 2000. He is currently a Professor with the Department of Electrical and Computer Engineering, University of Alberta, Edmonton, Alberta, Canada. He is a Fellow of the Engineering Institute of Canada. His research interests include real-time simulation of power systems and power electronic systems, electromagnetic transients, devicelevel modeling, large-scale systems, and parallel and distributed computing. computing.

Wenying Yang received the Ph.D. degree in electrical machinery and apparatus from the Harbin Institute of Technology, Harbin, China, in 2009. From August 2014 to August 2015, he was a Visiting Scholar with the University of Alberta, Edmonton, AB, Canada. He is currently an Professor with the Harbin Institute of Technology. His research interests include electrical numerical analysis, electromagnetic capability, and digital simulation and optimization of electromagnetic devices.